Test Statistic Auto- and Cross-correlation Effects on Monitor False Alert and Missed Detection Probabilities

Boris Pervan, Samer Khanafseh, and Jaymin Patel

Illinois Institute of Technology, Chicago, IL, USA

BIOGRAPHIES

Dr. Boris Pervan is a Professor of Mechanical and Aerospace Engineering at IIT, where he conducts research on advanced navigation systems. Prior to joining the faculty at IIT, he was a spacecraft mission analyst at Hughes Aircraft Company (now Boeing) and a postdoctoral research associate at Stanford University. Prof. Pervan received his B.S. from the University of Notre Dame, M.S. from the California Institute of Technology, and Ph.D. from Stanford University. He was the recipient of the IIT Sigma Xi Excellence in University Research Award, Ralph Barnett Mechanical and Aerospace Dept. Outstanding Teaching Award, Mechanical and Aerospace Dept. Excellence in Research Award, IIT University Excellence in Teaching Award, IEEE Aerospace and Electronic Systems Society M. Barry Carlton Award, RTCA William E. Jackson Award, Guggenheim Fellowship (Caltech), and the Albert J. Zahm Prize in Aeronautics (Notre Dame). He is an Associate Fellow of the AIAA, a Fellow of the Institute of Navigation (ION), and Editor-in-Chief of the ION Journal Navigation.

Dr. Samer Khanafseh is currently a Research Assistant Professor of Mechanical and Aerospace Engineering at IIT. He received his M.S. and PhD degrees in Aerospace Engineering from IIT, in 2003 and 2008, respectively. Dr. Khanafseh has been involved in several aviation applications such as Autonomous Airborne Refueling (AAR) of unmanned air vehicles, autonomous shipboard landing for NUCAS and JPALS programs and Ground Based Augmentation System (GBAS). His research interests are focused on high accuracy and high integrity navigation algorithms for close proximity applications, cycle ambiguity resolution, high integrity applications, fault monitoring and robust estimation techniques. He was the recipient of the 2011 Institute of Navigation Early Achievement Award for his outstanding contributions to the integrity of carrier phase navigation systems.

Jaymin Patel obtained his Bachelor's Degree in Mechatronics Engineering from Ganpat University in Mehsana, India in 2014.He is currently graduate student and Research Assistant in Mechanical And Aerospace Engineering at Illinois Institute of Technology (IIT). His current research focused on developing integrity monitors for the Ground Based Augmentation System (GBAS).

ABSTRACT

This paper investigates the influence of the autocorrelations of monitor test statistics over time and their cross-correlations across monitors on false alert and missed detection probabilities. General analysis methods are developed for the two problems. It is shown that cross-correlation across pairs of monitors directly influences the joint probability of missed detection, P_{MD}. This is in contrast to the effect of time auto-correlation, which primarily influences the probability of false alert, P_{FA}. The new methods are applied to the example problem of Ground Based Augmentation System (GBAS) ionospheric front monitoring.

INTRODUCTION

In this paper we analyze the effects on false alert and missed detection probabilities due to the autocorrelation of monitor test statistics over time and their cross-correlation across monitors. There has been some relevant earlier work on the effects of time correlation on false alert probabilities, as will be discussed below, but the scope was limited and the specific results were

not directly applicable any particular monitor. There has been no relevant prior work on the question of test statistic cross-correlation between monitors. The purpose of this paper is to fill these knowledge gaps.

In 2001, Brenner [1] used a direct Monte Carlo approach to demonstrate that the probability of false alert (P_{FA}) was higher than previously expected when a test statistic was time correlated and tested repeatedly over 15 sec, which is the specified GBAS continuity interval. Prior to Brenner's work, it was widely assumed that if the test statistic correlation time was large compared to the 15 sec interval, then the resulting P_{FA} would be nearly the same as if one independent test was executed over the interval. The results in [1] showed that this is not true, and in fact that P_{FA} can be much higher. However, the quantitative results of this early work were limited to the output of a first order filter with 100 sec time constant with input white noise, so they are not directly applicable any monitors, including GBAS ionospheric monitors of specific interest in the second half of this paper.

In 2003, Shively [2] confirmed Brenner's earlier results and provided an analytical upper bound on P_{FA} based on a linearized solution for the threshold-crossing problem in Papoulis [3]. Shively validated his analytical bound at several discrete points by direct Monte Carlo simulation and by comparison with the point results available in [1]. Shively's results were also limited to the output of a first order filter with a 100 sec time constant with input white noise.

In 2012, Rife [4] introduced a direct simulation approach to propagate the probability density function of a time-correlated test statistic over time. He showed that the existence of the constant threshold causes the distribution to quickly become non-Gaussian, even if the initial error distribution was Gaussian. The method is rigorous, but it has practical drawbacks: (1) the direct simulation is approximate, because the monitor density function needs to be discretized for time propagation, and (2) it is far too slow to use in a general analysis that may consider many different input stochastic models.

Concerning the influence of autocorrelation of test statistics over time, in this this paper, we

- generalize and tighten Shively's analytical P_{FA} bound, and correct a theoretical error in [2],
- develop new theory to quantify the impacts of autocorrelation of test statistics on P_{FA} and P_{MD},
- validate the new analytical methods using Monte Carlo simulations, and
- provide quantitative results for GBAS ionospheric front monitors.

In addition, we provide a new, general theory to quantify the influence on joint P_{MD} of cross-correlations of the outputs of any pair of monitors.

Monte Carlo simulations are used to directly validate the theory. Then the new analytical tools are used to generate useful quantitative results for GBAS ionospheric front monitors.

TEST STATISTIC AUTO-CORRELATION OVER TIME

To compute false alert probabilities for colored noise processes we use two methods:

1. a vectorized Monte Carlo method, which is more time-efficient than the direct simulations employed in [1], and
2. a theoretical approach to establish an upper bound on P_{FA}, which is a generalized version of the bound used in [2] .

While the first method (to be described shortly) is efficient by Monte Carlo standards, it is still far more time consuming than the theoretical method. Therefore the Monte Carlo method was mainly used to validate the theory, which, in turn, was used to generate most of the results in this paper. The theoretical bound, which is derived in Appendix A, is given by the two equations below:

$$P_{FA}(n, k_{FA}) \;=\; 1 - [1 - \; 2\Phi(-k_{FA})]\left\{1 - \frac{P_{\Delta}(k_{FA})}{1 - \; 2\Phi(-k_{FA})}\right\}^{n-1} \tag{1}$$

where,

$$P_{\Delta}(k) := \frac{1}{\pi} \exp\left(-\frac{k_{FA}^2}{2}\right) \operatorname{acos}\left[\frac{R_{YY}(\Delta t)}{R_{YY}(0)}\right] \tag{2}$$

and

- $\Phi(\blacksquare)$ is the cumulative distribution function (CDF) of the standard normal distribution
- k_{FA} is the normalized monitor threshold
- Δt is the sample interval
- n is the number of monitor tests in the exposure interval
- $R_{YY}(\blacksquare)$ is the autocorrelation function of the monitor output.

Shively [2] used a method similar to the one in Appendix A to derive a different analytical expression for P_{FA}. While that result was sufficient for the problem investigated in [2], namely the output of a first order 100-second filter with input white noise, it is not correct in the general case. It produces erroneous results for noise processes with long time constants – for example, if the same first order filter is fed by colored noise (e.g., due to multipath) rather than white noise. Equations (1) and (2) above provide correct results in all cases. This was verified by direct comparison with Monte Carlo simulation results, as discussed below.

The vectorized Monte Carlo method is outlined in the flow chart in Figure 1. In the following analysis we use 15 sec continuity exposure window (applicable to GBAS), and a sample interval of $\Delta t = 0.5$ sec, leading to $n = 30$. For simplicity, this figure shows how a single 30×1 white noise vector is processed. In actual implementation, m noise vectors can be processed simultaneously by inputting a $30\times m$ matrix instead. Figure 2 shows P_{FA} as a function of normalized threshold k_{FA} for a first order filter, with 100 sec time constant, subject to input white noise. This is the same case evaluated in references [1] and [2]. Theoretical results using equations (1) and (2) and vectorized Monte Carlo results are shown. Also included are three point results from [2], one theoretical and two from Monte Carlo simulation. The purpose of the figure is to help validate equations (1) and (2) by demonstrating the close correspondence between all of the results. The dashed line in this figure also shows the theoretically expected P_{FA} vs. k_{FA} under the assumption that there is only one independent test during the 15 sec exposure interval. It is obvious that the assumption is not valid—even though the filter time constant is much larger than 15 sec—and that its use would result in a significant underestimation of the actual false alert probability. The results also show that the vectorized Monte Carlo results match the point results from [2], and that the theoretical result upper bounds all of the Monte Carlo results.

Figure 3 shows the corresponding curves for the first order filter output given a colored multipath input: a first-order Gauss-Markov process with time constant $\tau_{mp} = 20$ sec. In this case, the theoretical result bounds the Monte Carlo result much more tightly, and the false alert probabilities are much closer to the single-sample curve than the previous white noise results (also shown in Figure 3). It is clear that the time constant of the input to the filter has a very strong influence on the false alert probability.

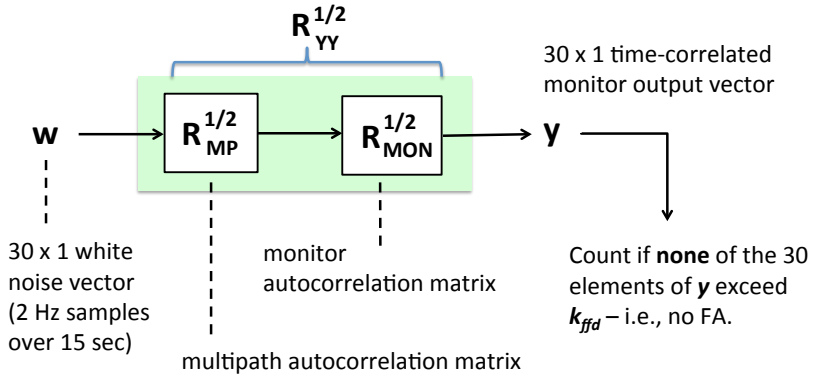

Figure 1. Flow Chart of the Vectorized Monte Carlo Process

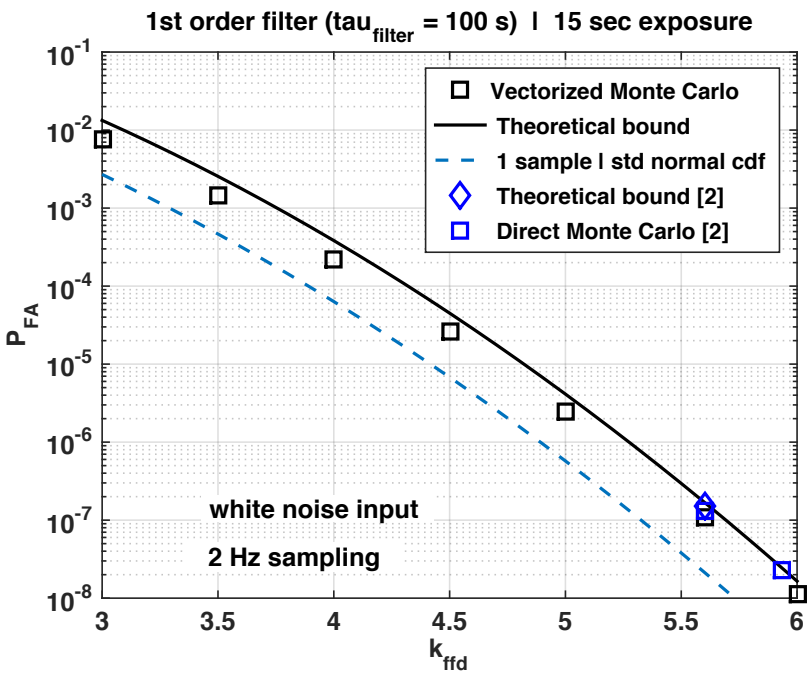

Figure 2: Comparison of New and Existing First Order Filter P_{FA} Results

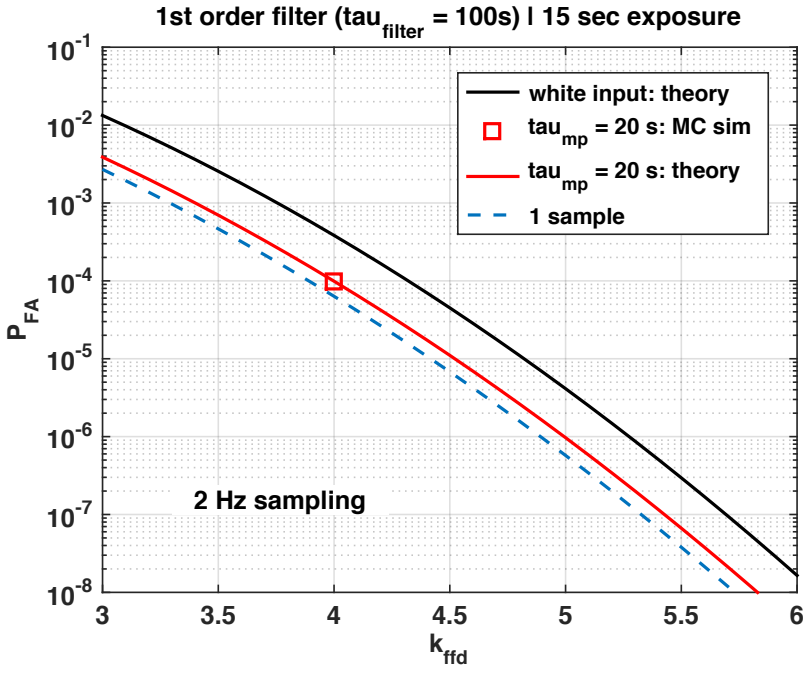

Figure 3: P_{FA} for First Order Filter with Multipath $\tau_{mp} = 20$ sec

Appendix A also provides the derivation of the following missed detection probability upper bound:

$$P_{MD}(n, k_{MD}) = \Phi(-k_{MD}) \left\{ 1 - \frac{P_{\Delta}(k_{MD})}{2\Phi(-k_{MD})} \right\}^{n-1} \tag{3}$$

where k_{MD} is the normalized integrity buffer. This bound was also validated by direct comparison with the results of vectorized Monte Carlo simulations (not shown here).

Note that $P_{FA}(1, k_{FA})$ and $P_{MD}(1, k_{MD})$ represent the *FA* and *MD* probabilities for a single monitor test. The effective numbers of independent samples in a given exposure time $n\Delta t$ for *FA* and *MD* are then, respectively,

$$n_{FA}(n, k_{FA}) = \log[1 - P_{FA}(n, k_{FA})] / \log[1 - P_{FA}(1, k_{FA})] \tag{4}$$

$$n_{MD}(n, k_{MD}) = \log P_{MD}(n, k_{MD}) / \log P_{MD}(1, k_{MD}). \tag{5}$$

TEST STATISTIC CROSS-CORRELATION ACROSS MONITORS

Evaluating the impact of test statistic cross-correlations between monitors involves additional considerations and requires different methods of analysis than the time autocorrelation case. On one extreme, for pairs of monitors that use mutually independent measurements, there would be no cross-correlation at all. Of course, not all cases are this easy. It is not uncommon that a given pair of monitors may use some, but not all, of the same measurements—and may use them differently in an attempt to detect the same fault. (Several examples relevant to GBAS will be given later in this paper.) The analysis of the influence of correlations between input measurements on the joint P_{MD} for two monitors is difficult, but it is necessary to ensure that the resulting integrity risk is properly overbounded. In Appendix B, we develop a general theory to quantify the impact of cross-correlations of the outputs of any pair of monitors.

EXAMPLE APPLICATION OF THE THEORY: GBAS IONOSPHERIC FRONT MONITORS

Here we will leverage the methods developed above (and in the Appendices) to produce quantitative results concerning time and monitor independence for the GBAS pseudorange Dual Solution Ionospheric Gradient Monitor (DSIGMA) and the airborne and ground-based Code Carrier Divergence (CCD) monitors. In Appendix C, it is shown that the transfer functions for the DSIGMA and CCD monitors are

$$Y_{dsig}(s) = \frac{s}{(\tau_1 s + 1)(\tau_2 s + 1)(\tau_{mp} s + 1)} N_{dsig}(s) \tag{6}$$

$$Y_{ccd}(s) = \frac{s}{(\tau_{ccd} s + 1)^2 (\tau_{mp} s + 1)} N_{ccd}(s) \tag{7}$$

where,

- N_{ccd} and N_{dsig} are white noise inputs,
- τ_{mp} is the time constant of errors entering the monitor (due to multipath),
- τ_1 and τ_2 are the DSIGMA time constants: 100 and 30 sec, respectively,

- τ_{ccd} is the CCD monitor time constant: 100 and 30 sec, respectively, for the air and ground versions of the monitor.

For comparison we can also write the first order filter transfer function that corresponds to the "monitors" used in [1] and [2] and to generate the results in Figures 2 and 3. Here we generalize to include the effects of input colored noise:

$$Y_f(s) = \frac{1}{(\tau_f s + 1)(\tau_{mp} s + 1)} N_f(s) \tag{8}$$

Note that equations (6) through (8) collapse to the case of a pure white noise input if we choose $\tau_{mp} = 0$.

Figure 4 shows the frequency responses (magnitudes only) of the individual ionospheric monitors. As shown in Appendix C the input to each of the three monitor models is raw GPS code-minus-carrier, which is heavily dominated by raw code phase error. It is significant that the monitors are all *band-pass* filters, meaning that monitor inputs at either extremely high or low frequencies will be rejected. This frequency selectivity suggests that accurate stochastic modelling of input error will be needed to obtain meaningful output results. Figures 5 through 7, respectively, show the corresponding curves for the first order filter and three IGM monitors given colored multipath inputs with an example time constant $\tau_{mp} = 20$ sec.

In Figures 8 through 10, we also present the results (for DSIGMA, airborne CCD, and ground CCD, respectively) in terms of the effective number of independent monitor tests during the 15 sec exposure interval – in this case for τ_{mp} ranging from 0 (white) to 100 sec. It is evident that the effective number of independent sample varies strongly with τ_{mp}. This is consistent with the expectations stated above based on the frequency response characteristics of the monitors. It is important to remember that τ_{mp} is the time constant of the *raw* (unsmoothed) pseudorange errors entering the monitor. (Carrier phase errors are negligible in comparison for all the monitors considered here.) There also is a somewhat weaker, but non-negligible, dependence on the normalized threshold k_{FA}.

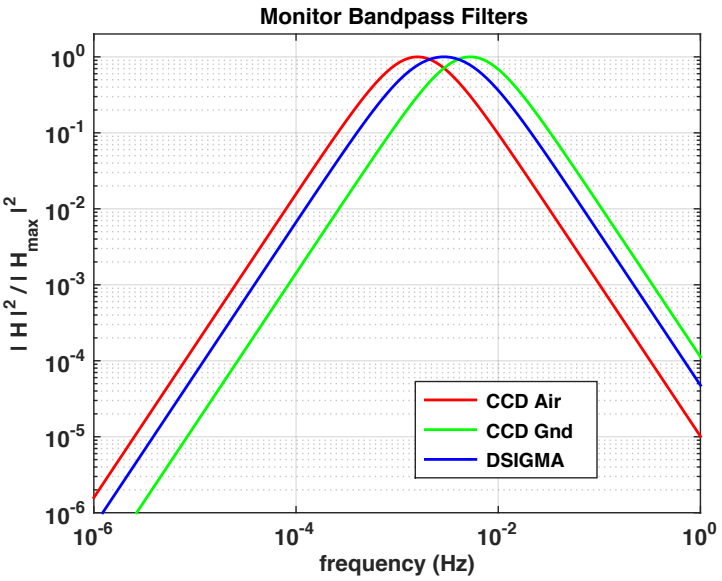

Figure 4: Monitor Frequency Responses

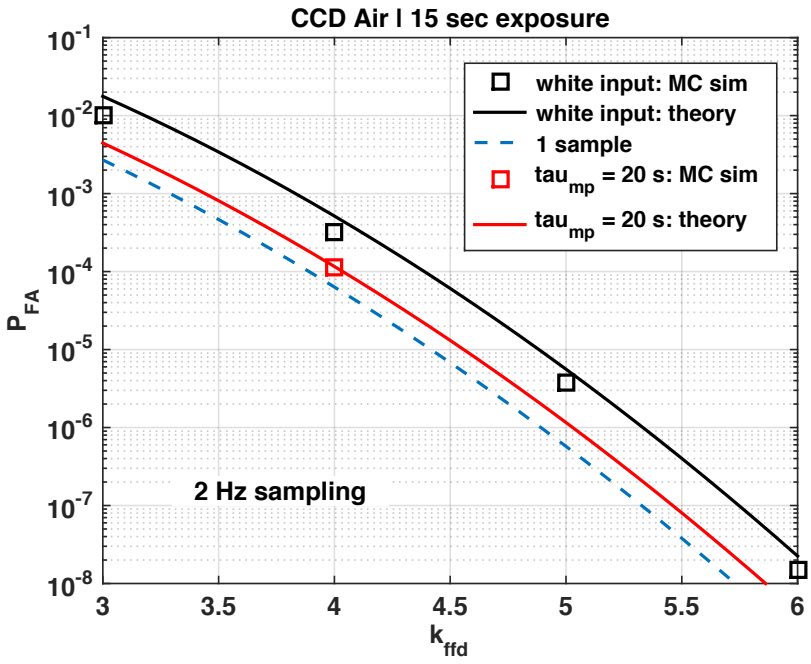

Figure 5: P_{FA} for CCD-Air Monitor with Multipath $\tau_{mp} = 20$ sec

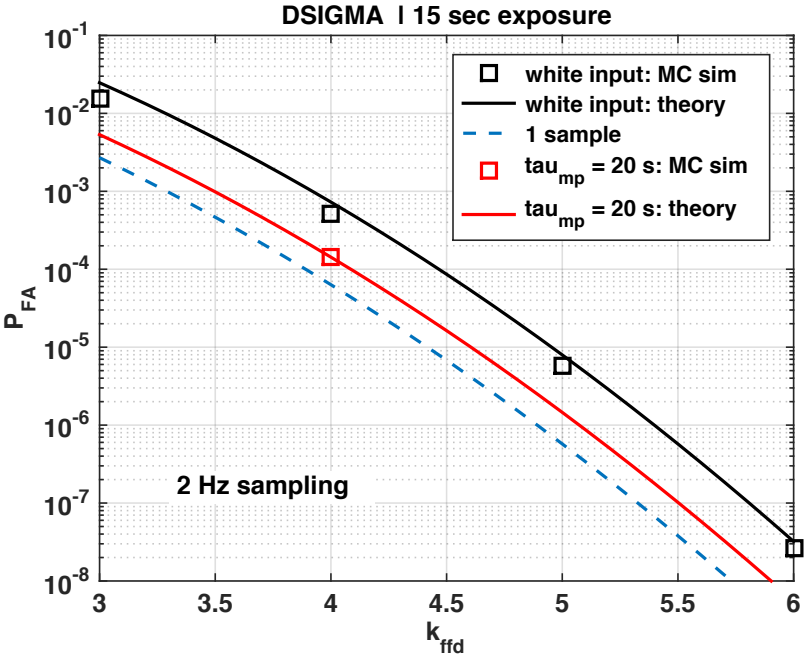

Figure 6: P_{FA} for DSIGMA Monitor with Multipath $\tau_{mp} = 20$ sec

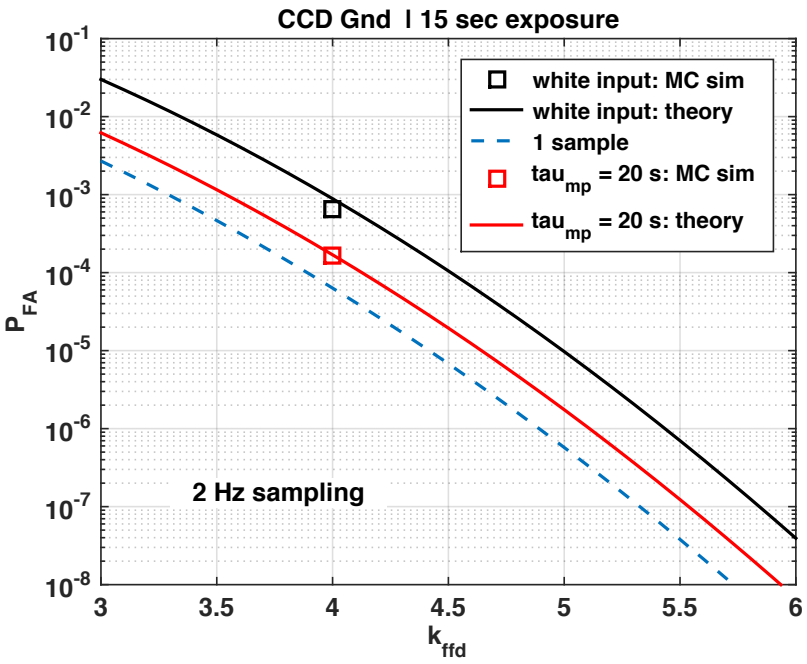

Figure 7: P_{FA} for CCD-Ground Monitor with Multipath $\tau_{mp} = 20$ sec

GBAS Multipath and Noise Autocorrelation Models

The Boeing Company and the Thales Group provided, respectively, the necessary airborne and ground data to create autocorrelation models for multipath and receiver noise. Raw code-minus-carrier autocorrelation data, with ionospheric effects removed, were used to generate the autocorrelation models described below. More detail on the data used to generate these models is provided in Appendix D.

Table 1 additionally shows the 5th, 50th (median), and 95th percentile time constants obtained from the Boeing and Thales experimental data. Given the finite amount of data available, it was not possible to reliably estimate time constants below the 5th and above the 95th percentiles. The especially large airborne time constant at the 95th percentile is caused by antenna group delay; this effect must in included in the airborne error model because it is an input error source which, like multipath and receiver noise, will influence the airborne monitor outputs.

Table 1: Monitor input autocorrelation model parameters

				τ time constant (sec)	
Percentile		**W_{MD}**	**W_{FA}**	**Boeing Air**	**Thales Ground**
(1)	< 5	0	0.05	0	0
(2)	5	0.05	0.45	7	6
(3)	50	0.45	0.45	14	7
(4)	95	0.50	0.05	170	13

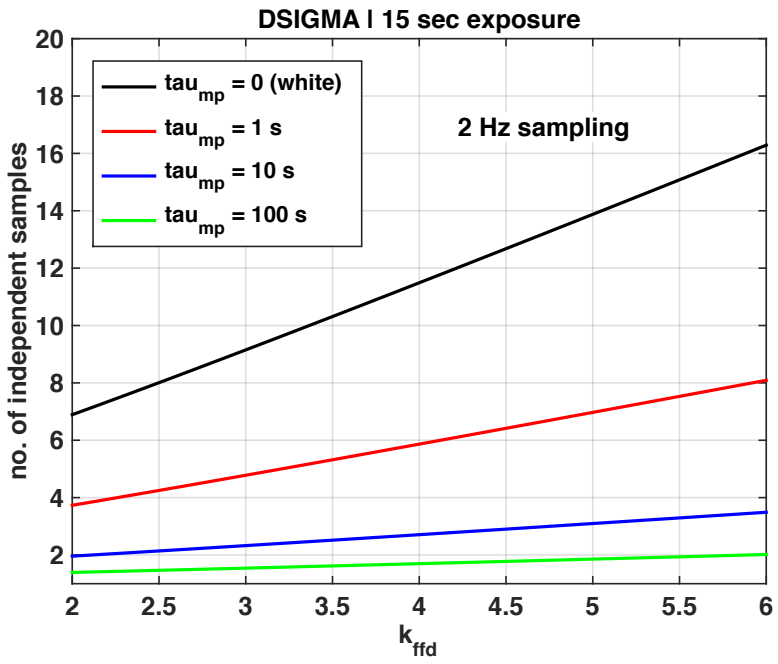

Figure 8: Effective Number of Independent Samples in 15 sec for DSIGMA Monitor

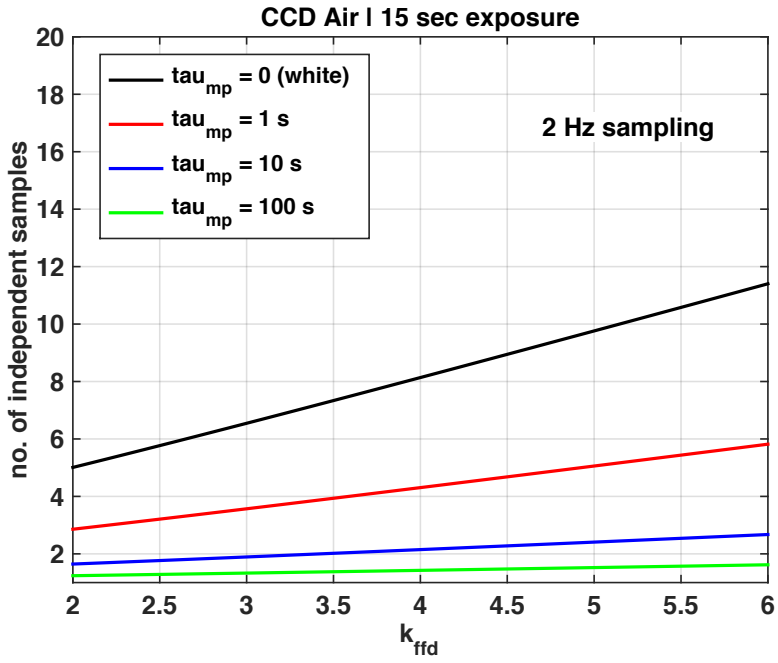

Figure 9: Effective Number of Independent Samples in 15 sec for CCD-Air Monitor

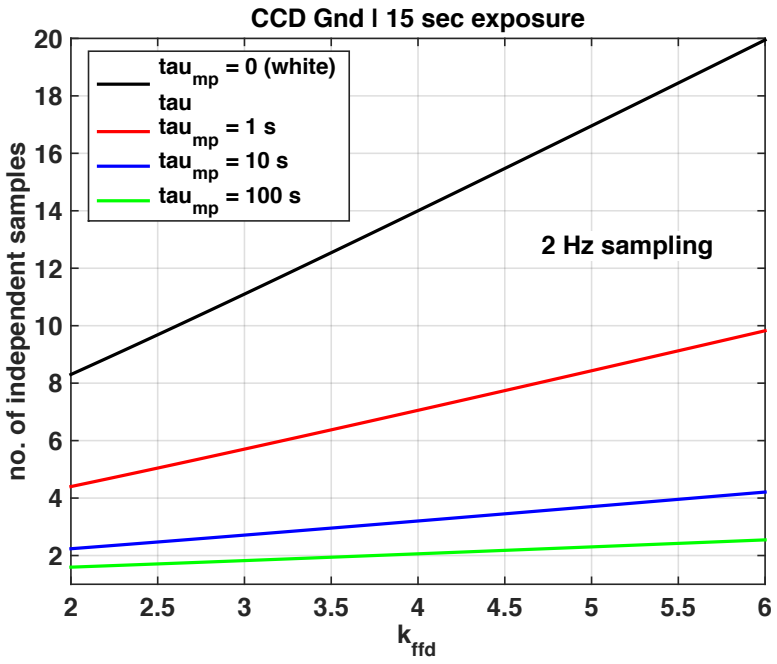

Figure 10: Effective Number of Independent Samples in 15 sec for CCD-Ground Monitor

The monitor *input* autocorrelation models for combined multipath and noise are:

$$R_{E,gnd}(t,i) \;=\; \sigma_{gnd}^2 \exp\left\{-|t| \,/\, \tau_{gnd}(i)\right\} \quad i \;= 1 \ldots 4 \tag{9}$$

$$R_{E,air}(t,i) \;=\; \sigma_{air}^2 \exp\left\{-|t| \,/\, \tau_{air}(i)\right\} \quad i \;= 1 \ldots 4 \tag{10}$$

where the air and ground multipath and noise errors are mutually independent, and the index i refers to the specific autocorrelation model in row (i) of Table 1. From the Boeing and Thales data in Appendix D, we also find that $\sigma_{air} =$ 0.40 m and $\sigma_{gnd} =$ 0.15 m are good approximations for the error standard deviations, regardless of satellite elevation.

The corresponding individual monitor *output* autocorrelation functions, $R_{E,DSIGMA}(t,i)$, $R_{E,CCD-G}(t,i)$, and $R_{E,CCD-A}(t,i)$, are then obtained using the monitor transfer functions in equations (6) and (7).

GBAS Nominal Ionospheric Error Models

The ground and air monitors will also be affected by nominal ionospheric divergence, which for an antenna at location x and time t is

$$\frac{dI(x,t)}{dt} = \frac{\partial I(x,t)}{\partial t} + \frac{\partial I(x,t)}{\partial x}\frac{dx}{dt} \tag{11}$$

Because we are concerned with *nominal* ionospheric effects, we assume that the derivatives above are constant over our spatial and temporal regions of interest. (Note that this does not mean that ionospheric errors are constant spatially or

temporally, just their derivatives.) Let v_F be the velocity of the nominal ionosphere relative to an observer fixed in reference frame *F*. In this case we have:

$$\dot{I}_F = \frac{\partial I}{\partial t} + v_F \frac{\partial I}{\partial x} \tag{12}$$

DSIGMA Monitor

The difference between nominal ionospheric divergence at the air and ground is

$$\Delta d := d_A - d_G := 2\left(\dot{I}_A - \dot{I}_G\right) \tag{13}$$

$$= 2(v_A - v_G)\frac{\partial I}{\partial x}$$

Note that $v_a - v_g$ is the velocity of the aircraft relative to the ground. For simplicity, we are free to assign $v_g = 0$. In terms of standard deviations, we may then write

$$\sigma_{\Delta d} = 2\, v_A\, \sigma_{VIG}\, F(\theta) \tag{14}$$

where σ_{VIG} is the standard deviation of the vertical ionospheric gradient and $F(\theta)$ is the obliquity factor for a satellite at elevation θ.

The resulting output response of the DSIGMA monitor is scaled by the difference in smoothing filter time constants: $\tau_1 - \tau_2 = 100\,\text{sec} - 30\,\text{sec} = 70\,\text{sec}$.

$$\sigma_{I,DSIGMA} = \sigma_{\Delta d}\,(\tau_1 - \tau_2) = 2\, v_A\, \sigma_{VIG}\, F(\theta)\,(\tau_1 - \tau_2) \tag{15}$$

where $\sigma_{I,DSIGMA}$ is the standard deviation of the nominal ionosphere contribution to the DSIGMA monitor test statistic. The aircraft velocity, v_a, during final approach varies between 135 and 290 knots [2]. We consider the following range of values for $\sigma_{VIG}, F(\theta)$, and v_A:

High:	$\sigma_{VIG} = 4\ \text{mm/km},$	$F(5°) \approx 3,$	$v_A = 290\ \text{knt}$
Low:	$\sigma_{VIG} = 1\ \text{mm/km},$	$F(90°) = 1,$	$v_A = 135\ \text{knt}$

This results in a range of possible values for $\sigma_{I,DSIGMA}$:

$$0.01\text{m} < \sigma_{I,DSIGMA} < 0.25\ \text{m}.$$

CCD-Air and Ground Monitors

For the CCD-Ground monitor the nominal input divergence is simply

$$d_G = 2\,\dot{I}_G = 2\frac{\partial I}{\partial t} \tag{16}$$

The monitor measures divergence directly so $\sigma_{I,CCD-G} = \sigma_{d_G}$. Based on experimental data collected in CONUS, reference [3] recommends the use of $\sigma_{d_G} = 4\ \text{mm/s}$. Therefore, in this analysis, for the CCD-Ground monitor we use

$$\sigma_{I,CCD-G} \;=\; 4 \text{ mm/s}.$$

The nominal ionospheric divergence seen by the CCD-Air monitor is

$$d_A = 2\,\dot{I}_A \;=\; 2\left(\frac{\partial I}{\partial t} \;+\; v_A\,\frac{\partial I}{\partial x}\right) =\; d_G + 2\,v_A\,\frac{\partial I}{\partial x} \tag{17}$$

which leads to the following nominal ionospheric contribution (standard deviation) to the monitor test statistic

$$\sigma_{I,CCD-A} \;=\; \sigma_{d_A} \;=\; \sqrt{\sigma_{d_G}^2 + 4\,v_A^2\,F(\theta)^2\sigma_{VIG}^2} \tag{18}$$

Considering again the same range of values for σ_{VIG}, $F(\theta)$, and v_a results in a range of possible values for $\sigma_{I,CCD-A}$:

$$4 \text{ mm/s} \;<\; \sigma_{I,CCD-A} \;<\; 5.4 \text{ mm/s}.$$

Nominal Ionosphere Autocorrelation Model

Because we assume that the nominal ionospheric derivatives are constant over our spatial and temporal regions of interest, we have the following autocorrelation function for the monitor output due to nominal ionospheric effects:

$$R_{I,MON}(t) = \sigma_{I,MON}^2 \quad \forall \quad t \in [0,T] \tag{19}$$

where $[0,T]$ is our time interval of interest, and *'MON'* can be any of the three monitors above.

Composite Monitor Output Autocorrelation Model

The nominal ionospheric and multipath/noise contributions to the monitor outputs are independent. Therefore the corresponding output autocorrelation functions are:

$$\begin{aligned} R_{DSIGMA}(t,i) \;&=\; R_{E,DSIGMA}(t,i) \;+\; R_{I,DSIGMA}(t) \\ R_{CCD-G}(t,i) \;&=\; R_{E,CCD-G}(t,i) \;+\; R_{I,CCD-G}(t) \\ R_{CCD-A}(t,i) \;&=\; R_{E,CCD-A}(t,i) \;+\; R_{I,CCD-A}(t) \end{aligned} \tag{20}$$

Results: GBAS Ionospheric Front Monitor Test Statistic Auto-Correlation Over Time

To estimate P_{FA} and P_{MD} we use a weighted composite of the four input multipath and noise models in Table 1:

$$P_{FA}(n,k_{FA}) = \textstyle\sum_{i=1}^{4} P_{FA}(n,i,k_{FA})\,W_{FA}\,(i) \tag{21}$$

$$P_{MD}(n, k_{MD}) = \sum_{i=1}^{4} P_{MD}(n, i, k_{MD})\, W_{MD}\,(i) \tag{22}$$

where $W_{FA}(i)$ and $W_{MD}(i)$ are the weighting factors assigned to the specific autocorrelation models in row (i) of Table 1, and for a given autocorrelation model i, $P_{FA}(n, i, k_{FA})$ and $P_{MD}(n, i, k_{MD})$ are computed using equations (1) and (3), respectively. To help obtain upper bound estimates of P_{FA} and P_{MD} the weighting factors were selected to emphasize the lower time constants for P_{FA} and higher time constants for P_{MD}.

Based on the DSIGMA and CCD-Air monitor P_{MD} results, it is safest to assume low-nominal ionospheric conditions, corresponding to scenarios where multipath and noise have increased influence. These are the blue curves in Figures 11 and 12. For the CCD-Ground monitor in Figure 13 there is only one nominal ionospheric model, so there is only one curve. The CCD-Ground monitor has a lower filter time constant than CCD-Air, and the input multipath contributions also have lower time constants on the ground than in the air. For these reasons, the CCD-Ground monitor has more (effectively) independent samples during a 15 sec continuity interval. However, both of these monitors are much more heavily influenced by nominal ionospheric effects than DSIGMA, which leads to an even larger number of independent samples (for DSIGMA) than for either of the other two monitors.

For a typical normalized threshold $k_{FA} = 5.5$ and a 15 sec continuity interval, we can safely, and with margin, assume 5 independent samples for DSIGMA, 2 for CCD-Air, and 3 for CCD-Ground.

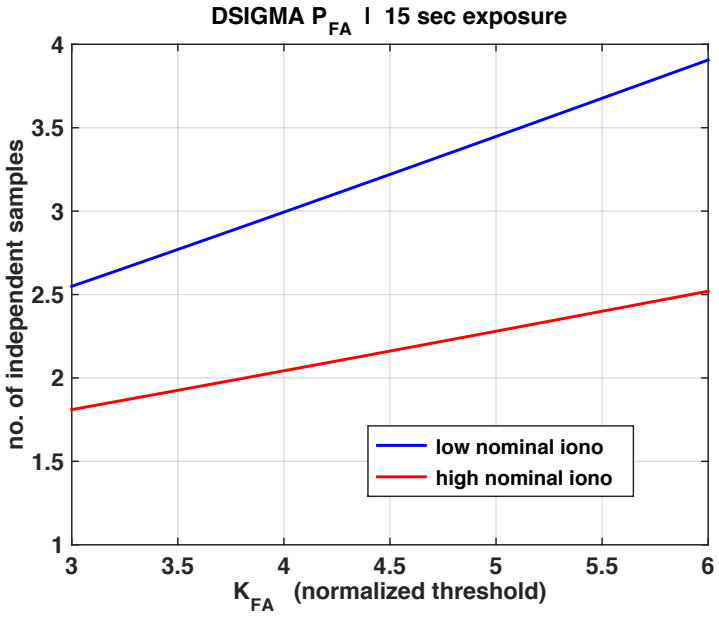

Figure 11: Effective Number of P_{FA} Independent Samples for DSIGMA Monitor

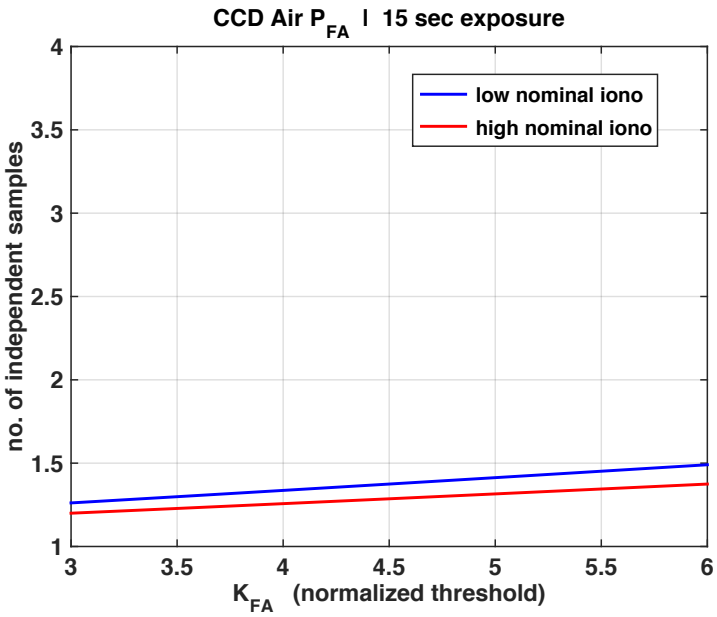

Figure 12: Effective Number of P_{FA} Independent Samples for CCD-Air Monitor

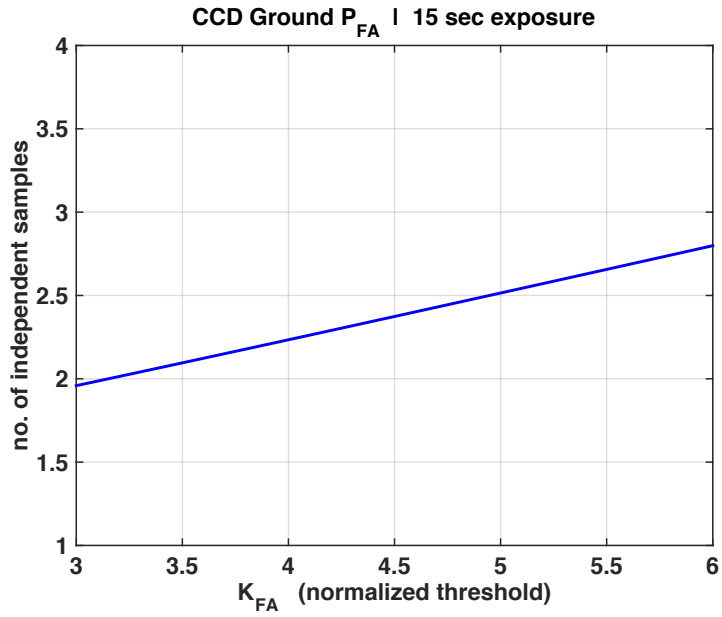

Figure 13: Effective Number of P_{FA} Independent Samples for CCD-Ground Monitor

The DSIGMA, CCD-Air, and CCD-Ground P_{MD} results, shown in Figures 14 through 17, indicate that more than one independent sample can only be assumed if the ionospheric front is nearly static from the monitor's point of view. This is

especially true for CCD-Air and -Ground, where the results suggest that it is safest to assume a single monitor sample, even for fronts that appear static to the monitors for longer than 10 minutes. However, two independent samples can be assumed for the DSIGMA monitor for ionosphere fronts that appear static to the DSIGMA monitor for a period of at least 5 minutes.

Results: GBAS Ionospheric Front Monitor Test Statistic Cross-Correlation Between Monitors

The new results are shown in Figures 17 through 19. Figure 17 shows the cross-correlation impact between the CCD-Air and DSIGMA monitors. The CCD-Air monitor is dominated by nominal ionospheric divergence, whereas the DSIGMA monitor mainly by multipath and noise. However both monitors are additionally influenced by nominal ionospheric gradients. For the low-level nominal gradient the monitors are essentially decorrelated, but at the high nominal gradient limit there is substantial correlation. Still, even in the latter case, an order of magnitude reduction in P_{MD} exists relative to either monitor alone, at least for $k_{md} \geq 3.5$.

Figure 18 shows the cross-correlation impact between the CCD-Ground and DSIGMA monitors. This case is the same as the previous one, except that the CCD-Ground monitor is not affected by nominal ionospheric gradients. The existence of a higher ionospheric gradient affects only the DSIGMA monitor in this case, causing even further decorrelation between the two monitors. The P_{MD} results in the Figure 18 show that these two monitors are essentially independent.

The correlation between the CCD-Ground and Air monitors is much more significant, because both monitors are heavily dominated by nominal ionospheric divergence. The results in the Figure 19 clearly indicate that P_{MD} credit can only be taken for one of these monitors.

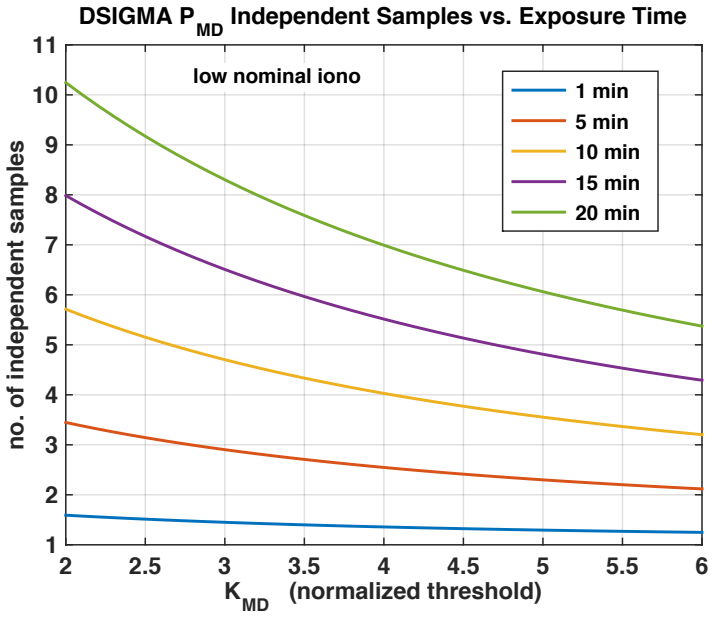

Figure 14: Effective Number of P_{MD} Independent Samples for DSIGMA Monitor

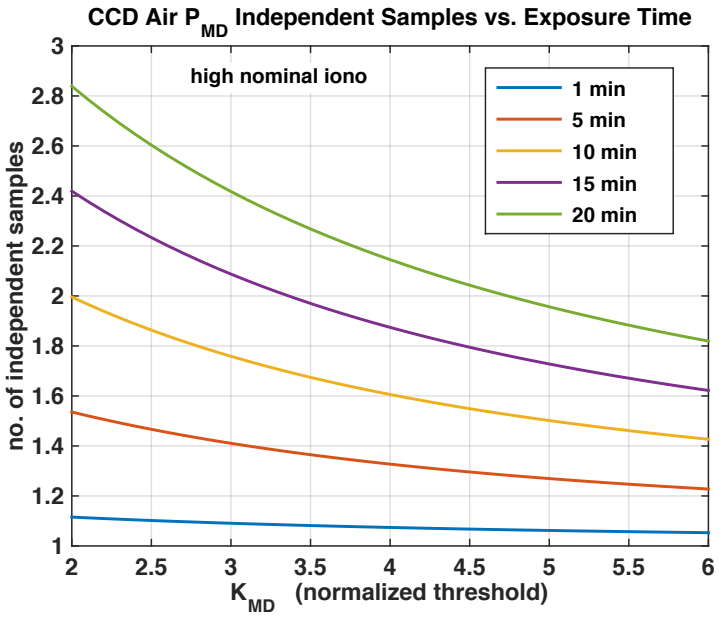

Figure 15: Effective Number of P_{MD} Independent Samples for CCD-Air Monitor

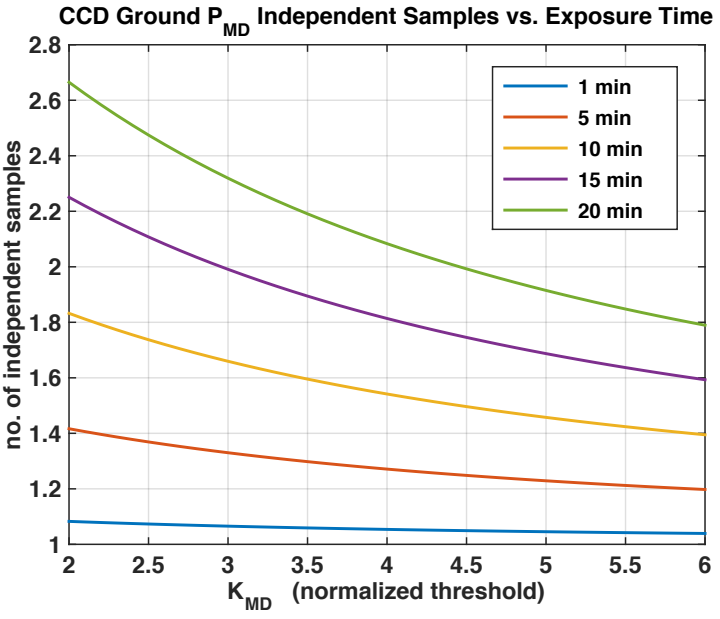

Figure 16: Effective Number of P_{MD} Independent Samples for CCD-Ground Monitor

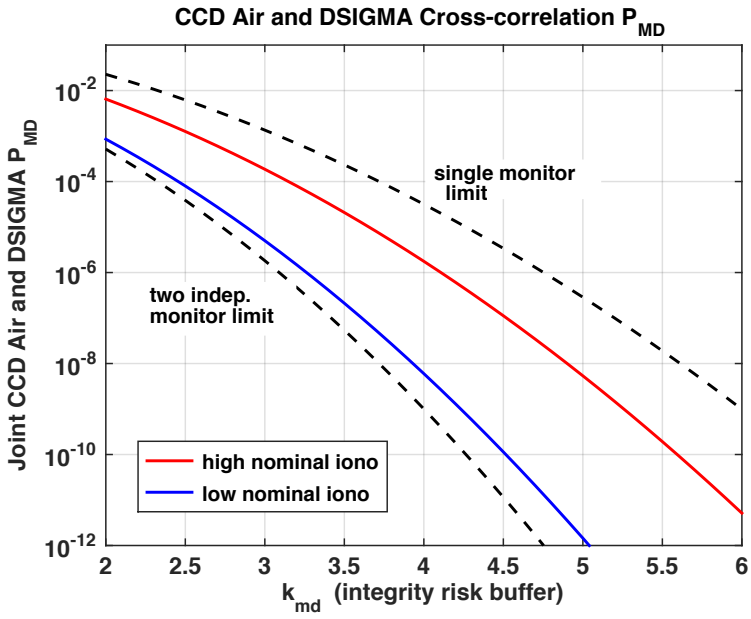

Figure 17: Joint P_{MD} for DSIGMA and CCD-Air

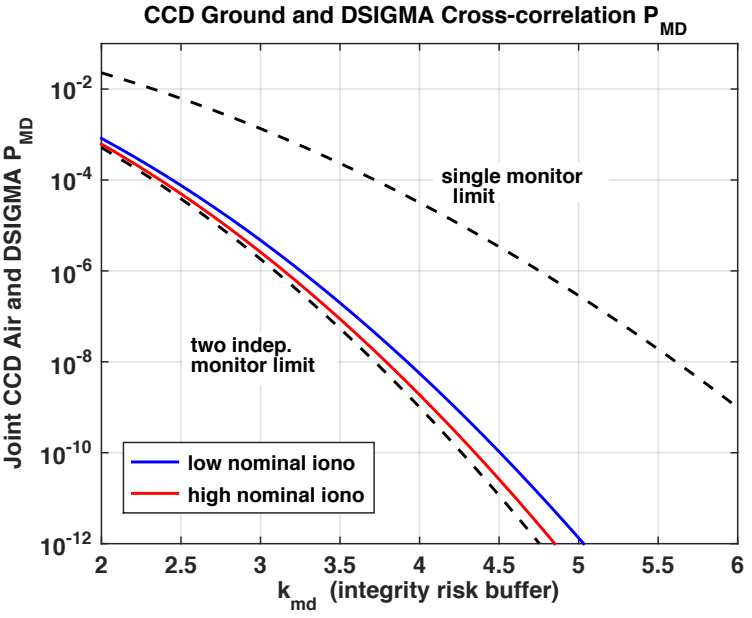

Figure 18: Joint P_{MD} for DSIGMA and CCD-Ground

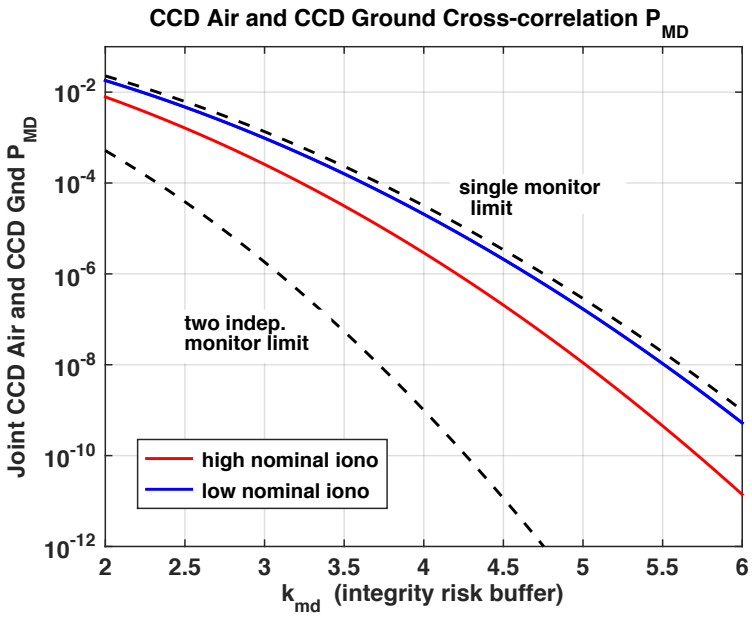

Figure 19: Joint P_{MD} for CCD-Air and CCD-Ground

A Note on the GBAS Ground-Based Ionospheric Gradient Monitor (IGM)

Any discussion of GBAS ionospheric monitors would be incomplete without mention of ground-based Ionospheric Gradient Monitors (IGM), like those described in [5] and [6]. These use input carrier phase measurements, so the multipath and noise errors affecting them will be essentially independent from those affecting the CCD-Air, CCD-Ground and DSIGMA monitors—because the multipath and noise in the latter monitors are dominated by code phase errors. In addition, nominal ionospheric gradient effects on the IGM, which could otherwise cause some correlation with CCD-Air and DSIGMA test statistics, are heavily dominated by nominal tropospheric turbulence [5]. Tropospheric turbulence also overshadows the effects of the carrier phase multipath and noise. For all these reasons, we may safely assert that the IGM output will be statistically independent from the outputs of the other three monitors.

However, understanding IGM test statistic time correlation requires knowledge and data available today only to ground system providers, so no analysis is possible. Therefore, without specific design details, it is recommended that conservative assumptions be used – namely, that

1. the maximum number of independent samples over 15 sec be assumed the for P_{FA}– e.g., $15\ \mathrm{sec}/\Delta t$ samples – and

2. the minimum number of independent samples per an approach be assumed for P_{MD}– e.g., one independent sample per approach.

CONCLUSION

This paper investigated the influence of the autocorrelations of monitor test statistics over time and their cross-correlations across monitors on false alert (FA) and missed detection (MD) probabilities. General analysis methods are developed for the two problems. It is shown that cross-correlation across pairs of monitors directly influences the joint probability of missed detection, P_{MD}. This is in contrast to the effect of time auto-correlation, which primarily influences the probability of false

alert, P_{FA}. The new methods are applied to a specific example: Ground Based Augmentation System (GBAS) ionospheric front monitoring.

Concerning the effects of *auto-correlation over time* on P_{FA}, it was shown that for DSIGMA and CCD-Air, it is safest to assume low-nominal ionospheric conditions, corresponding to scenarios where multipath and noise dominate. The CCD-Ground monitor has a lower filter time constant than CCD-Air, and the input multipath contributions also have lower time constants on the ground than in the air (due to aircraft antenna group delay). For these reasons, the CCD-Ground monitor has more (effectively) independent samples during a 15 sec continuity interval. Still, both of these monitors are much more heavily influenced by nominal ionospheric effects than is DSIGMA, which leads to an even larger number of independent samples for DSIGMA than either of the other monitors. It was shown that for a typical normalized monitor threshold of $k_{FA} = 5.5$ and a 15 sec exposure, we can safely, and with margin, assume 5 independent samples for DSIGMA, 2 for CCD-Air, and 3 for CCD-Ground.

The DSIGMA, CCD-Air, and CCD-Ground P_{MD} results, showed that only one independent sample must be assumed unless the ionospheric front is present and nearly static, from the monitor's point of view, for a long period of time. This is especially true for CCD-Air and CCD-Ground, where the results suggest that it is safest to assume a single monitor sample even for fronts that appear static to the monitors for well over 10 minutes. Two independent samples may be assumed for the DSIGMA monitor for ionosphere fronts that appear static to the monitor for a period of at least 5 minutes.

New results for *cross-correlation between monitors* were also presented. The CCD-Air monitor is dominated by nominal ionospheric divergence, whereas the DSIGMA monitor mainly by multipath and noise. Both monitors are additionally influenced by nominal ionospheric gradients. For low-level gradients the two monitors are essentially decorrelated, but there is substantial correlation at the high nominal gradient limit. Still, even in the latter case, an order of magnitude reduction in P_{MD} exists relative to using either monitor alone. The cross-correlation case between the CCD-Ground and DSIGMA monitors is similar, except that the CCD-Ground monitor is not affected by nominal ionospheric gradients. The existence of a higher ionospheric gradient affects only the DSIGMA monitor in this case, causing even further decorrelation between the two monitors. The P_{MD} results showed that these two monitors are essentially independent. In stark contrast, the CCD-Ground and Air Monitors are highly correlated because both monitors are heavily dominated by nominal ionospheric divergence. The results showed that P_{MD} credit may only be taken for one of these monitors.

Finally, it was concluded based on the independent dominating error sources, that the ground-based IGM output is statistically independent from the outputs of DSIGMA, CCD-Air, and CCD-Ground. With regard to IGM time auto-correlation, performance specifics may vary widely between ground system providers. For this reason, it is recommended to conservatively assume the maximum number of independent samples over 15 sec for P_{FA} and the minimum number of independent samples (one) per approach for P_{MD}.

ACKNOWLEDGEMENTS

The authors thank Matt Harris (Boeing) and Andre Schuettpelz (Thales) for generously providing the autocorrelation data in Appendix D and Shelly Beauchamp and Christopher Wolf at the Federal Aviation Administration (FAA) for supporting this research. However, the views and opinions expressed in this paper are those of the authors alone and do not necessarily reflect the opinions of any other organization or person.

REFERENCES

[1] Brenner, M., "Concern Regarding Mean Time Between Trials for a Smoothed Signal," *RTCA SC-159/WG-4/30*, August 16, 2001.

[2] Shively, C., and Varner, C., "Impact of Carrier Smoothing on Event Probabilities in LAAS," *Proceedings of ION 58th Annual Meeting,* Albuquerque, NM, June 24-26, 2002.

[3] Papoulis, A., *Probability, Random Variables, and Stochastic Processes*, McGraw-Hill, 1965.

[4] Rife, J., and Misra, P., "Impact of Time-Correlation of Monitor Statistic on Continuity of Safety-Critical Operations," *NAVIGATION: Journal of The Institute of Navigation*, Vol. 59, No. 4, Winter 2012.

[5] Reuter, R., Weed, D., and Brenner, M., "Ionosphere gradient detection for Cat III GBAS," *Proceedings of the 25th International Technical Meeting of the Satellite Division of the Institute of Navigation* (ION GNSS 2012), Nashville, TN, Sept. 2012.

[6] Jing, J., Khanafseh, S., Langel, S., Chan, F.-C., and Pervan, B., "Optimal Antenna Topologies for Spatial Gradient Detection in Differential GNSS," *Radio Science*, Vol. 50, Issue 7, July 2015.

APPENDICES

Appendix A: Derivation of Probability of Threshold Crossing

Definitions:

NC → acronym for "No Crossing,"
C → acronym for "Crossing"
A_i → an *event*: "test statistic above threshold at time index i"
B_i → an *event*: "test statistic below threshold at time index i"

The probability that all n test statistics are below the threshold is

$$P(B_1, \dots, B_n) = P(B_1) \prod_{i=2}^{n} P(B_i \mid B_{i-1})$$

where

$$P(B_i \mid B_{i-1}) = \frac{P(B_i, B_{i-1})}{P(B_{i-1})}$$

and

$$P(B_i) = P(B_i, B_{i-1}) + P(B_i, A_{i-1})$$

which is the same as

$$P(B_i, B_{i-1}) = P(B_i) - P(B_i, A_{i-1})$$

Combining the equations above we have

$$P(B_1, \dots, B_n) = P(B_1) \prod_{i=2}^{n} \frac{P(B_i) - P(B_i, A_{i-1})}{P(B_{i-1})}$$

We assume that the sensor error process is stationary over the time interval of interest, i.e., n consecutive samples, so that

$$P(B_1) = P(B_i) = P(B_{i-1}).$$

The probability of crossing a threshold at $\pm k$ is

$$P_\Delta(k) := P(B_i, A_{i-1}) = P(A_i, B_{i-1}) = \frac{1}{\pi} \exp\left(-\frac{k^2}{2}\right) \operatorname{acos}\left[\frac{R_{MON}(\Delta t)}{R_{MON}(0)}\right].$$

The result above, which is the same as equation (2), can be derived by following Papoulis's treatment of the *level crossing problem* in [7], and combining separate intermediate results on pages 486 and 492 of [7]. The 'level' here is the normalized threshold k. The expression is accurate when $R_{MON}(\Delta t)/R_{MON}(0)$ is close to 1, which is true for all of the auto-correlation analysis in this work. Numerous point probability results have been verified by direct Monte Carlo simulation for all monitors analyzed in this work.

Now consider the false alert case, where we have two thresholds at $\pm k$. In this case

$$P_{FA}(n,k) \;=\; 1 - P(B_1, \ldots, B_n) \;=\; P(B_1)\left\{\frac{P(B_1) - P_\Delta(k)}{P(B_1)}\right\}^{n-1}$$

and then

$$P_{FA}(n,k_{FA}) \;=\; 1 - [1 - \; 2\Phi(-k_{FA})]\left\{1 - \frac{P_\Delta(k_{FA})}{1 - \; 2\Phi(-k_{FA})}\right\}^{n-1}$$

which is the same as the false alert probability expression in equation (1).

For the missed detection problem a fault exists, so we are concerned with crossing one threshold, either k or $-k$, based on the sign of the fault. We assume the probability of crossing the other threshold will be negligibly small when a fault is present. Therefore, for no threshold crossing assuming a one-sided threshold

So for a fault a constant distance d above the threshold, the missed detection probability is

$$P_{MD}(n,d) \;=\; P(B_1, \ldots, B_n) \;=\; P(B_1)\left\{\frac{P(B_1) - P_\Delta(d)/2}{P(B_1)}\right\}^{n-1}$$

Considering the case where $d = k_{MD}$

$$P_{MD}(n,k_{MD}) \;=\; \Phi(-k_{MD})\left\{1 - \frac{P_\Delta(k_{FA})}{2\Phi(-k_{MD})}\right\}^{n-1}$$

which is the same as the missed detection probability in equation (3).

Appendix B: Monitor Cross-Correlation Theory

We will consider the cross correlation between a pair of arbitrary monitors defined by

$$Y_1(s) \;=\; M_1(s)\, U_1(s)$$
$$Y_2(s) \;=\; M_2(s)\,[\, U_1(s) + \; U_2(s)\,]$$

where $M_1(s)$ and $M_2(s)$ are the transfer functions of the two monitors, and $Y_1(s)$ and $Y_2(s)$ are the respective monitor outputs. The measurement error input to the first monitor is $U_1(s)$. The second monitor also accepts input $U_1(s)$, but has an

additional input $U_2(s)$, which is statistically independent from $U_2(s)$. Because the inputs to the two monitors are obviously correlated, the outputs will, in the general case, also be correlated.

In general, the independent input contributions $U_1(s)$ and $U_2(s)$ may individually be correlated over time. We can model such time correlations by passing white noise inputs through error model filters:

$$\begin{aligned} U_1(s) &= W_1(s)\, N_1(s) \\ \mathrm{U_2(s)} &= \mathrm{W_2(s)\, N_2(s)} \end{aligned}$$

where $W_1(s)$ and $W_2(s)$ are the colored error filters for the two monitor inputs, and $N_1(s)$ and $N_2(s)$ are white noise processes with unit power spectral density.

We can now write

$$\boxed{\begin{aligned} Y_1(s) &= \bar{M}_1(s)\, N_1(s) \\ Y_2(s) &= Y_{21}(s) + Y_{22}(s) \\ Y_{21}(s) &= \bar{M}_{21}(s)\, N_1(s) \\ Y_{22}(s) &= \bar{M}_{22}(s)\, N_2(s) \end{aligned}}$$

where

$$\begin{aligned} \bar{M}_1(s) &= M_1(s)\, W_1(s) \\ \bar{M}_{21}(s) &= M_2(s)\, W_1(s) \\ \bar{M}_{22}(s) &= M_2(s)\, W_2(s) \end{aligned}$$

We can also express the boxed equations as systems of differential equations (in time) in state space form:

$$\begin{aligned} \dot{x}_1 &= F_1\, x_1 + G_1\, n_1 \\ y_1 &= H_1\, x_1 \end{aligned}$$

$$\begin{aligned} \dot{x}_{21} &= F_{21}\, x_{21} + G_{21}\, n_1 \\ y_{21} &= H_{21}\, x_{21} \end{aligned}$$

$$\begin{aligned} \dot{x}_{22} &= F_{22}\, x_{22} + G_{22}\, n_2 \\ y_{22} &= H_{22}\, x_{22} \end{aligned}$$

$$y_2 = [\, H_{21}\ H_{22}\,] \begin{bmatrix} x_{21} \\ x_{22} \end{bmatrix}$$

These can be combined into a single state space system as follows:

$$\dot{x} = Fx + Gn$$

where

$$x = \begin{bmatrix} x_1 \\ x_{21} \\ x_{22} \end{bmatrix}, \quad F = \begin{bmatrix} F_1 & 0 & 0 \\ 0 & F_{21} & 0 \\ 0 & 0 & F_{21} \end{bmatrix}, \quad G = \begin{bmatrix} G_1 & 0 \\ G_{21} & 0 \\ 0 & G_{22} \end{bmatrix}, \quad \text{and} \quad H = \begin{bmatrix} H_1 & 0 & 0 \\ 0 & H_{21} & H_{22} \end{bmatrix}$$

Now let us define X and Y as the covariance matrices of vectors x and y, respectively. Recalling that the power spectral densities are both 1, the covariance propagation equation is

$$\dot{X} = FX + XF^T + GG^T$$

Assuming the monitor filters are in steady state with respect to the noise inputs, we have

$$0 = FX_{ss} + X_{ss}F^T + GG^T$$

This is a Lyapunov Equation, which can be solved for X_{ss} (for example, by using the *lyap* function in Matlab®). In turn we can then obtain the steady state covariance matrix of the vector y,

$$Y_{ss} = HX_{ss}H^T$$

which is the covariance matrix of the joint distribution of the outputs of the two monitors

$$y = \begin{bmatrix} y_1 \\ y_2 \end{bmatrix} \sim N_y\,(0, Y_{ss})$$

Finally, the joint missed detection probability can be written as

$$P_{MD}(k_{md}) = P(\,y_1 > k_{md} \cap\, y_2 > k_{md}) = \int_{k_{md}}^{\infty}\int_{k_{md}}^{\infty} N_y\,(0, Y_{ss})\; dy_1\, dy_2$$

The integral for the bivariate Gaussian distribution has no general analytic solution, so it must be evaluated numerically. (This can be done efficiently by using the Matlab® function *mvncdf*.)

Appendix C: Derivation of Monitor Transfer Functions

Definitions:

- k is the time index
- Δt is the sample interval
- N is an integer number of samples used to define the filter gain
- τ is the time constant of the smoothing filter
- p is the raw pseudorange
- $\bar{p}$ is the smoothed pseudorange
- ϕ is the carrier phase (expressed in the same length units as p)

DSIGMA

The standard GBAS smoothing filter is:

$$\bar{p}(k) = \frac{N-1}{N}\left[\,\bar{p}(k-1) + \phi(k) - \phi(k-1)\right] + \frac{1}{N}p(k)$$

This can be expressed in continuous time form (using a backward difference approximation for time differentiation) as

$$\tau\dot{\bar{p}}(t) + \bar{p}(t) = \tau\dot{\phi}(t) + p(t)$$

where $\tau = N/\Delta t$. Taking the Laplace Transform gives

$$\bar{P}(s) = \frac{\tau s\Phi(s) + P(s)}{\tau s + 1} = \frac{\tau s}{\tau s + 1}\Phi(s) + \frac{1}{\tau s + 1}P(s)$$

The DSIGMA monitor takes the difference of two such filters with different time constants:

$$\begin{aligned} \mathcal{Y}_{dsig}(s) &= \left(\frac{\tau_1 s}{\tau_1 s + 1} - \frac{\tau_2 s}{\tau_2 s + 1}\right)\Phi(s) + \left(\frac{1}{\tau_1 s + 1} - \frac{1}{\tau_2 s + 1}\right)P(s) \\ &= \frac{\tau_1 s(\tau_2 s + 1) - \tau_2 s(\tau_1 s + 1)}{(\tau_1 s + 1)(\tau_2 s + 1)}\Phi(s) + \frac{(\tau_2 s + 1) - (\tau_1 s + 1)}{(\tau_1 s + 1)(\tau_2 s + 1)}P(s) \\ &= \frac{(\tau_1 - \tau_2)s}{(\tau_1 s + 1)(\tau_2 s + 1)}\Phi(s) - \frac{(\tau_1 - \tau_2)s}{(\tau_1 s + 1)(\tau_2 s + 1)}P(s) \\ &= \frac{(\tau_2 - \tau_1)s}{(\tau_1 s + 1)(\tau_2 s + 1)}[P(s) - \Phi(s)] \end{aligned}$$

Under normal error conditions (no ionospheric front), $P(s) - \Phi(s)$ can be replaced by the difference in the *errors* between the two measurements, $E_{P-\Phi}(s)$. This, in turn is almost completely dominated by the multipath and noise on the raw pseudorange $P(s)$. (Note that the differentiator, s, in the numerator of the transfer function eliminates the carrier phase cycle ambiguity.)

If we model the raw pseudorange error as a first order Gauss Markov Random Process (GRMP), i.e., white noise passed though a first order filter, we have the following false output from the DSIGMA monitor:

$$\mathcal{Y}_{dsig}(s) = \frac{s}{(\tau_1 s + 1)(\tau_2 s + 1)(\tau_{mp} s + 1)} \cdot (\tau_2 - \tau_1)\sqrt{2\tau_{mp}(\sigma_p^2 + \sigma_\phi^2)} \cdot N_{dsig}(s)$$

where $N_{dsig}(s)$ is input white noise with unit power spectral density. When normalized by its standard deviation, the output of the DSIGMA monitor is

$$Y_{dsig}(s) = \frac{\mathcal{Y}_{dsig}(s)}{(\tau_2 - \tau_1)\sqrt{2\tau_{mp}(\sigma_p^2 + \sigma_\phi^2)}} = \frac{s}{(\tau_1 s + 1)(\tau_2 s + 1)(\tau_{mp} s + 1)} N_{dsig}(s)$$

CCD

The CCD monitor differences pseudorange minus carrier over time and passes the result through two identical first order filters in series. Following the methods above, the output error can be expressed in terms of the input error and the filter transfer function:

$$E_{ccd}(s) = \frac{s}{(\tau_{ccd} s + 1)^2}E_{P-\Phi}(s)$$

The differentiator, s, in the numerator accounts for the time differencing of the input, and τ_{ccd} is the time constant of the monitor's two filters.

As in the DSIGMA case, we note that under normal error conditions the input error is almost entirely due to the raw pseudorange, which we model again as a first order GMRP. The result is:

$$y_{ccd}(s) = \frac{s}{(\tau_{ccd}s+1)^2(\tau_{mp}s+1)} \cdot \sqrt{2\tau_{mp}(\sigma_p^2+\sigma_\phi^2)} \cdot N_{ccd}(s)$$

In normalized form, the output is:

$$Y_{ccd}(s) = \frac{y_{ccd}(s)}{\sqrt{2\tau_{mp}(\sigma_p^2+\sigma_\phi^2)}} = \frac{s}{(\tau_{ccd}s+1)^2(\tau_{mp}s+1)} \cdot N_{ccd}(s)$$

Note that the CCD monitor transfer function has the same general form as that DSIGMA transfer function, except that the filter time constants are different.

Appendix D: Ground and Airborne Experimental Data

The Boeing Company and the Thales Group provided airborne and ground data to create autocorrelation models for multipath and receiver noise. Raw code-minus-carrier data, with ionospheric effects removed, was used generate the autocorrelation models.

Boeing 787 Aircraft Flight Data

Figure 20 shows the sample means and standard deviations binned by satellite elevation. The results suggest that it is reasonable to assume zero mean and standard deviation of 0.4 m for all elevations.

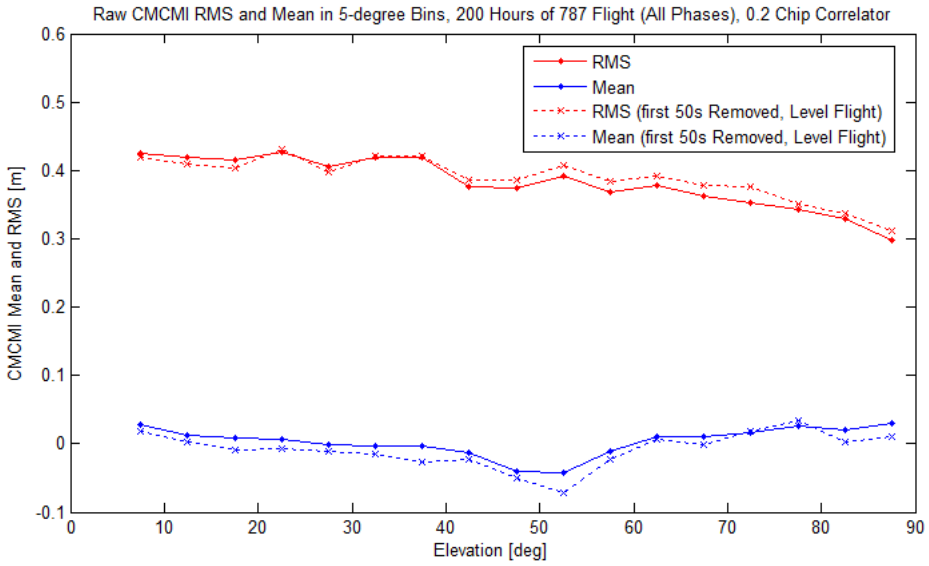

Figure 20: Airborne Mean and Standard Deviation

Figure 21 shows a composite of autocorrelation traces of the flight data. A number traces with long correlation times are clearly evident; these are caused by antenna group delay, and must be accounted for in the autocorrelation model.

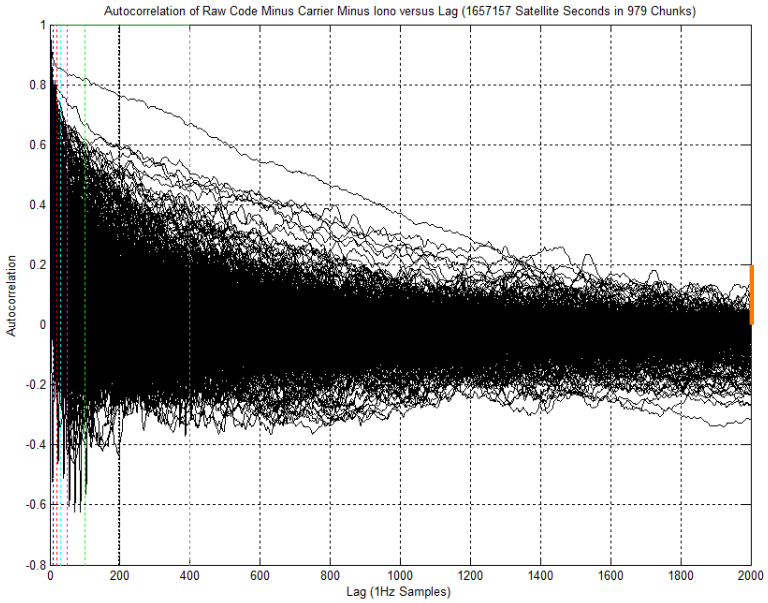

Figure 21: Airborne Autocorrelation Traces

Figure 22 consolidates the autocorrelation data into empirical cumulative distribution functions for a number of discrete lag times.

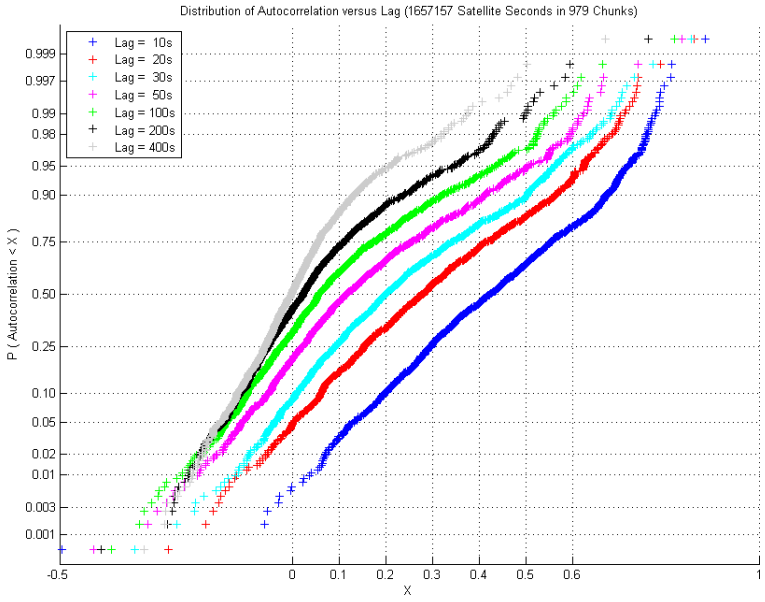

Figure 22: Airborne Autocorrelation Distributions at Various Lag Times

To make subsequent time and monitor independence analyses tractable, the autocorrelation data is then further consolidated in Figure 23 into three models, corresponding to the 5th, 50th and 95th percentile autocorrelation functions.

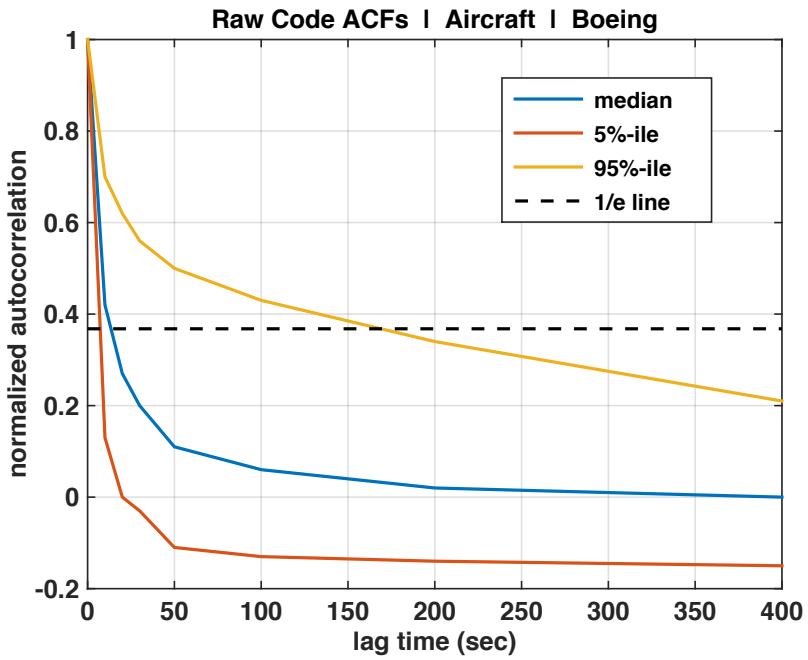

Figure 23: 5th, 50th, and 95th Percentile Airborne Autocorrelation Functions

Thales GBAS Ground Facility Data

Figure 24 shows the sample means and standard deviations binned by satellite elevation. The results suggest that it is reasonable to assume zero mean and standard deviation of 0.15 m for all elevations.

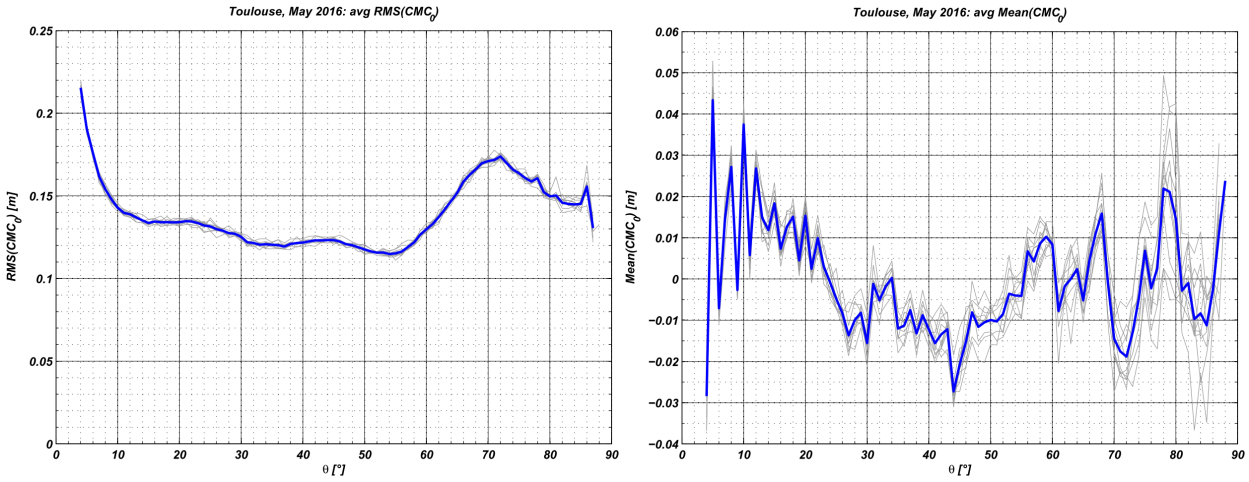

Figure 24: Ground Mean and Standard Deviation

Figure 25 shows a composite of autocorrelation traces of the ground data. Note that group-delay-induced long correlation times (present in the airborne data) do not exist here.

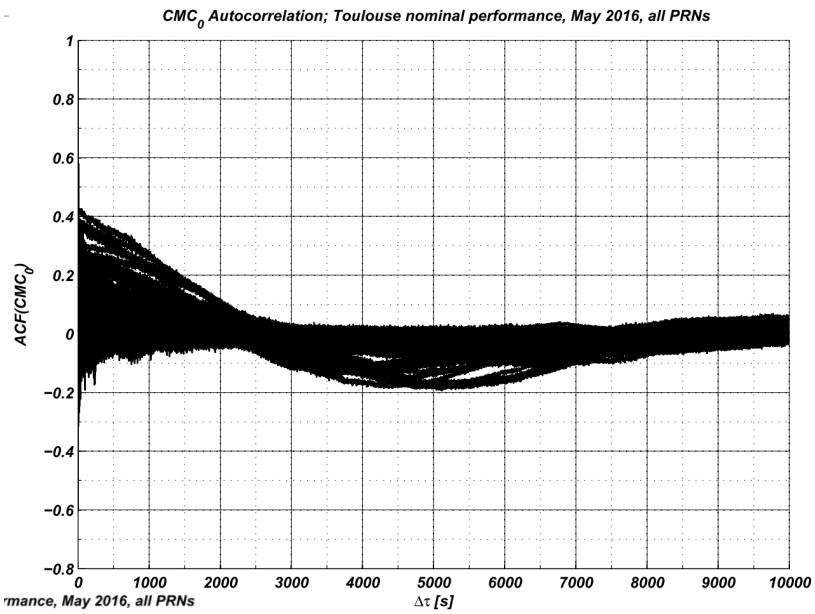

Figure 25: Ground Autocorrelation Traces

Figure 26 consolidates the autocorrelation data into empirical distribution functions at a number of discrete lag times.

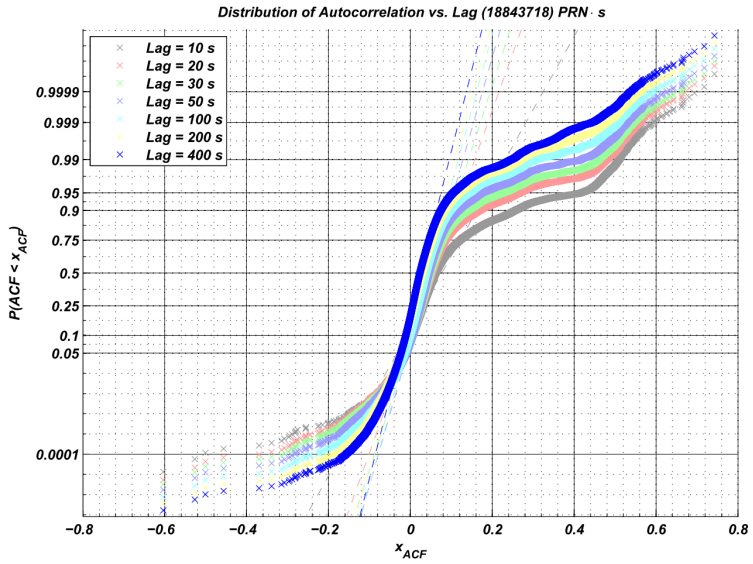

Figure 26: Ground Autocorrelation Distributions at Various Lag Times

For use in the time and monitor independence analysis, the autocorrelation data is then further consolidated in Figure 27 into three models, corresponding to the 5th, 50th and 95th percentile autocorrelation functions.

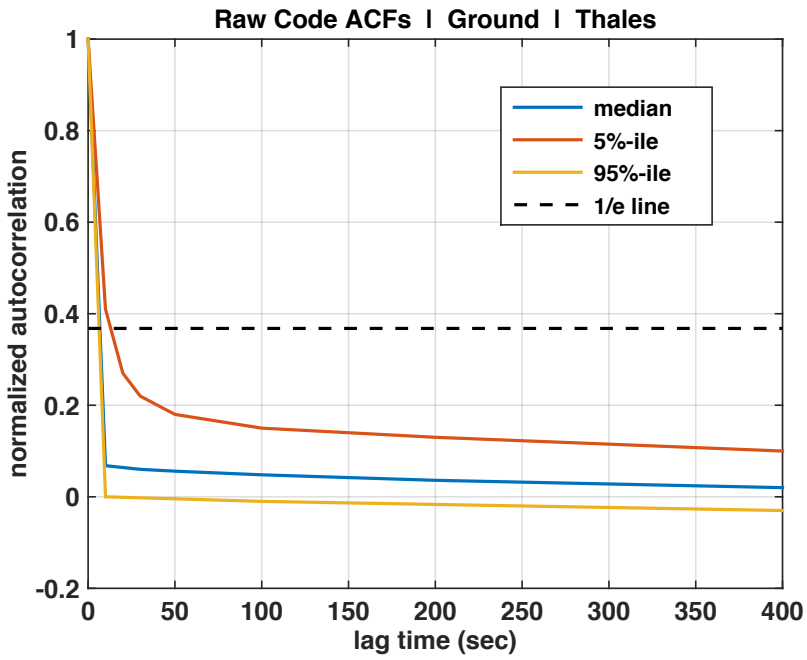

Figure 27: 5th, 50th, and 95th Percentile Ground Autocorrelation Functions